Prediction of dendritic spacings in a directional-solidification experiment

James A. Warren*

Department of Physics, University of California, Santa Barbara, California 93106-4030

J. S. Langer

Institute for Theoretical Physics, University of California, Santa Barbara, California 93106-4030
(Received 10 August 1992; revised manuscript received 12 October 1992)

We present a theoretical analysis of the formation of a dendritic array in a directional-solidification experiment. Our calculation contains three sequential ingredients: acceleration of an initially flat interface and the concomitant buildup of a solutal boundary layer in front of it; onset of a morphological instability, triggered by thermal fluctuations, producing a relatively finely spaced array of dendritic tips; coarsening of this array and final selection of a steady-state primary spacing. For sufficiently large growth speeds, where the resulting dendrites interact with each other weakly, we find—with no adjustable parameters—good agreement with the experiments of Trivedi and Somboonsuk [Acta Metall. **33**, 1061 (1985)] and Somboonsuk, Mason, and Trivedi [Metall. Trans A **15A**, 967 (1984)].

I. INTRODUCTION

Prediction of the primary spacing of dendrites in the mushy zone of a solidifying alloy is among the most important unsolved problems in the theory of microstructural pattern formation. To date the most carefully controlled laboratory studies relevant to this problem have been observations of dendritic arrays formed in the directional solidification of thin films of experimentally convenient substances such as succinonitrile. The most detailed work along these lines has been that of Somboonsuk and Trivedi (referred to hereafter as TS for Ref. [1] and SMT for Ref. [2]). Our purpose in this paper is to report on a detailed theoretical analysis of their results.

In an earlier investigation, we carried out a stability analysis for the final, steady-state, dendritic arrays observed by SMT. We found that, at large enough pulling speeds where we expected our analysis to be valid, a finite range of primary spacings was allowed, and the observed spacings were well within the predicted region of stability. From this we concluded that the actual spacing observed in any experiment must depend on the detailed way in which the sample is prepared and set in motion; that is, that dendritic spacings of this special class of experimental situations must be history dependent.

Accordingly, we present here a step-by-step analysis of the sequence of events leading to the final, steady-state configuration observed in the SMT experiments. This sequence is best described by reference to a set of photographs that appears in TS and is reproduced here as Fig. 1. The system consists of a thin film of succinonitrile plus 5.5% molar (4.0 wt %) acetone, contained between glass plates, and pulled to the left through a fixed temperature gradient so that solidification appears to take place from left to right. Initially the system is at rest and the liquid-solid interface is flat. The pulling mechanism is then turned on abruptly, and the following events take place.

(1) The temperature decreases at the position of the interface, that is, the solidification front moves backward relative to the temperature gradient. In order to remain in local thermodynamic equilibrium at this lower temperature, solidification begins to take place and a boundary
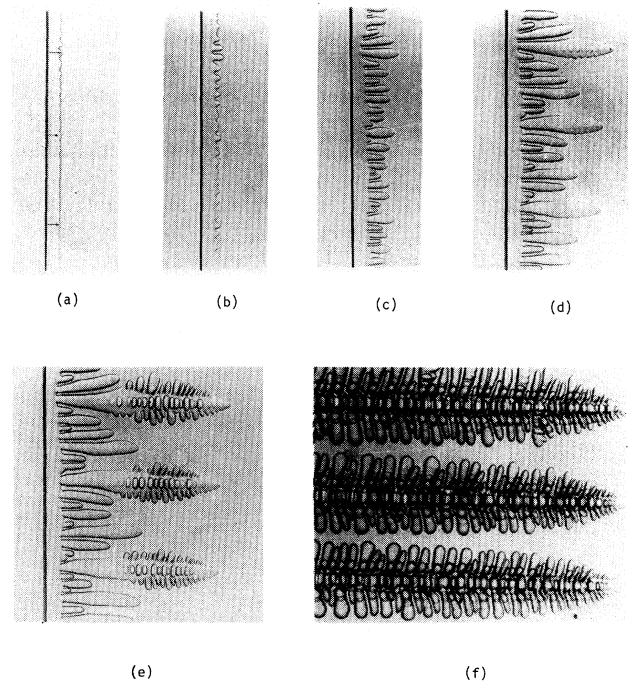

FIG. 1. Sequence of photographs taken from TS illustrating the instability of a planar interface and the subsequent development of a steady-state dendritic array. (Reprinted from R. Trivedi and K. Somboonsuck, Acta Metall. **33**, 1061, copyright 1985, with permission from Pergamon Press Ltd., Headington Hill Hall, Oxford OX3 0BW, U.K.)

layer of rejected impurities begins to form ahead of the front.

(2) As solidification accelerates, the front undergoes a Mullins-Sekerka instability seen in Figs. 1(a) and 1(b). The wavelength λ_0 at which this instability first appears, seen clearly in Fig. 1(b), was found by TS to be about an order of magnitude larger than predicted by the conventional Mullins-Sekerka analysis for a front moving at the pulling speed. TS deduced from this observation that the instability must be occurring while the front is still moving relatively slowly.

(3) At the point at which the instability becomes visible (its amplitude becomes roughly comparable to its wavelength), the forward-pointing bulges already look much like an array of dendritic tips, and the motion of the front apparently has entered a strongly nonlinear regime. These dendritic tips now undergo a coarsening instability, that is, they go through a stage of competitive growth in which tips that fall behind their neighbors are overgrown and eventually eliminated from the final array. This process is occurring in Figs. 1(c) and 1(d).

(4) The spacing reaches its steady-state value λ_1 well before the dendrites themselves are fully developed, as seen in Fig. 1(e). The resulting regular array of tips finally accelerates to the pulling speed. The steady-state array is shown in Fig. 1(f).

Our analysis deals quantitatively with each of these stages of the process. In Sec. II we develop a simple model to describe the initial acceleration of the flat solidification front and its concomitant buildup of the boundary layer of impurities ahead of it. Section III is devoted to an analysis of the Mullins-Sekerka instability during this initial transient. Here we compute the way in which the instability is triggered by fluctuations, and we verify the TS conjecture that the instability goes all the way into its nonlinear regime at relatively long wavelengths while the interface is still moving quite slowly. In Sec. IV we present a model of the subsequent coarsening instability. This model is a generalization of our earlier analysis of the competitive interactions between dendritic tips; it is used here to compute how the system moves from the initial spacing λ_0 to a final, steady-state spacing λ_1. When we put together all of these ingredients, without any adjustable parameters, we obtain values of λ_1 that are consistent to within 20% with the experimental observations of SMT.

II. MOTION OF THE FLAT INTERFACE

We start by defining our notation and specifying the various approximations to be used in our analysis. The solidifying material, a dilute solution of acetone in succinonitrile, is contained between glass plates, with separations in the range 50–500 μm. Because λ_1 is of the same order of magnitude as the plate separation; our process (at least in its later stages) is effectively two dimensional. We assume that hydrodynamic motion can be neglected and that all transport of solute is diffusive. In addition, the latent heat of fusion is assumed to be sufficiently small and the thermal conductivities of the liquid and solid sufficiently large and close to one another that the temperature throughout the system is determined by the applied temperature gradient G. We define our coordinate system so that

$$T = T_0 + Gz \, , \tag{2.1}$$

and, in accord with the assumptions stated in the previous sentence, understand that this relationship is independent of the position or shape of the solidification front. The variable z measures displacement parallel to the direction of motion in a frame moving at the pulling speed v_p with respect to the solidifying material. In what follows we refer to this frame of reference as the "gradient frame." The temperature T_0 is the melting temperature of the pure material. Note that, because the tips of the dendrites must be undercooled, this choice of position for $z = 0$ means that the entire solidification front is always in the region $z < 0$.

The specific experimental substance with which we compare our theoretical results is the weak solution of 5.5% molar acetone in succinonitrile used by SMT. We assume that this solution is sufficiently dilute that we can make linear approximations for the liquidus and solidus in the equilibrium phase diagram. The quantities m and m' are, respectively, the slopes (dT/dc) of the liquidus and solidus. The symbol c denotes the concentration of the solute; and the ratio $m/m' = K < 1$ is the partition coefficient. The initial concentration of the liquid, that is, the concentration infinitely far ahead of the solidification front, is $c_\infty = 0.055$. We also assume that solutal diffusion in the solid is much slower than diffusion in the liquid and can therefore be neglected.

With the above definitions and assumptions, the equation which governs the evolution of our system is simply the equation for solute diffusion in the liquid. In the gradient frame, this is

$$D \frac{\partial c_0^2}{\partial z^2} + v_p \frac{\partial c_0}{\partial z} = \frac{\partial c_0}{\partial t} \, , \tag{2.2}$$

where $c_0(z,t)$ is the time-dependent concentration field ahead of the planar front. There are several boundary conditions which must be satisfied. Assuming local equilibrium at the boundary, we require

$$c_0(z_0,t) = -\frac{G}{m} z_0 \, , \tag{2.3}$$

where z_0 is the position of the interface in the gradient frame. The velocity of the interface in the frame of reference that is fixed in the solidifying material (hereafter referred to as the "material frame"), is

$$v_0(t) = v_p + \dot{z}_0(t) \, . \tag{2.4}$$

Finally, conservation of solute at the interface requires

$$D \frac{\partial c_0}{\partial z} \bigg|_{z_0} = v_0(1 - K)c_0(z_0,t) \, . \tag{2.5}$$

In principle, we must solve the system of equations (2.2)–(2.5) for fixed $v_p > 0$ and initial conditions appropriate to the stationary interface at $v_p = 0$. That is,

$$c_0(z,0)=\begin{cases}c_\infty, & z>z_0(0)\\ Kc_\infty, & z<z_0(0) \ .\end{cases} \tag{2.6}$$

We know of no exact analytic solution of this version of the Stefan problem. Rather than resorting to extensive numerical techniques, we propose a relatively simple boundary-layer approximation that appears adequate for our purposes. Note that in steady-state the concentration profile ahead of a flat interface moving at the pulling speed is

$$c_p(z)=c_\infty+\left[\frac{c_\infty}{K}-c_\infty\right]e^{-2(z-z_\infty/K)/l_p} \ , \tag{2.7}$$

where the diffusion length l_p is

$$l_p=\frac{2D}{v_p} \ , \tag{2.8}$$

and z_∞, the steady-state position of the planar interface in the gradient frame, is

$$z_\infty=-\frac{m}{G}c_\infty \ . \tag{2.9}$$

Remember that, in steady state, the concentration of the liquid at the interface is c_∞/K, and the concentration in the solid is c_∞. The second term on the right-hand side of (2.7) describes the boundary layer of excess solute that moves ahead of the interface.

With (2.7) in mind, it seems plausible to assume that the non-steady-state concentration profile can be approximated by a function of the form

$$c_0(z,t)=c_\infty+[c_0(z_0,t)-c_\infty]e^{-2(z-z_0)/l} \ , \tag{2.10}$$

where l is now a time-dependent parameter describing the thickness of the boundary layer, and $z_0(t)$ is the instantaneous position of the interface. Behind the interface, in the solid where no diffusion occurs, the concentration is $c(z<z_0)=Kc(z=z_0(t))$. We see that this approximation correctly describes both the initial and final states of our system; that is, $l=0$ and $c(z_0,t=0)=c_\infty$ correspond to the initial state, and $l=2D/v_p$ and $c(z_0,t=\infty)=c_\infty/K$ correspond to the final state.

Our strategy now is to use the ansatz (2.10) to derive equations of motion for z_0 and l. Equation (2.5) combined with (2.10) implies

$$v_0(1-K)c_0(z_0,t)=\frac{2D}{l}[c_0(z_0,t)-c_\infty] \ . \tag{2.11}$$

Integration of the diffusion equation (2.2) from z_0 to ∞ yields

$$-D\frac{\partial c_0}{\partial z}\bigg|_{z=z_0}+v_0[c_\infty-c_0(z_0,t)]$$

$$=\frac{\partial}{\partial t}\int_{z_0}^\infty dz'c(z',t) \ , \tag{2.12}$$

which, with (2.10) and (2.5), gives

$$v_0[c_\infty-Kc_0(z_0,t)]=\frac{\partial}{\partial t}\left[\frac{l[c_0(z_0,t)-c_\infty]}{2}\right] \ . \tag{2.13}$$

Finally, using the local equilibrium condition (2.3) we obtain

$$v_0(t)=v_p+\dot z_0=\frac{2D(z_0-z_\infty)}{l(1-K)z_0} \ , \tag{2.14}$$

and

$$\dot l=\frac{4D(z_\infty-Kz_0)}{l(1-K)z_0}-\frac{l}{z_0-z_\infty}\dot z_0 \ . \tag{2.15}$$

A numerical solution of Eqs. (2.14) and (2.15) is shown in Fig. 2 in the form of a trajectory in the z_0,l plane. Relevant parameters are $G=67$ K/cm and $v_p=10$ μm/s. For small times t, it is easy to show analytically that

$$l\approx\left[\frac{8Dt}{3}\right]^{1/2} \ , \tag{2.16}$$

and

$$z_0=z_\infty-v_pt+\frac{v_p\sqrt{2D}}{\sqrt{3}|z_\infty|(1-K)}t^{3/2} \ . \tag{2.17}$$

Note that the initial motion in the material frame is proportional to $t^{3/2}$. The most prominent feature of Fig. 2 is its oscillatory approach to steady state, which occurs for all pulling speeds greater than $v_p\approx0.024$ μm/s. We believe this oscillation is a physically realistic effect, not an artifact of our approximation scheme. On the other hand, for pulling speeds greater than about 10 μm/s, this
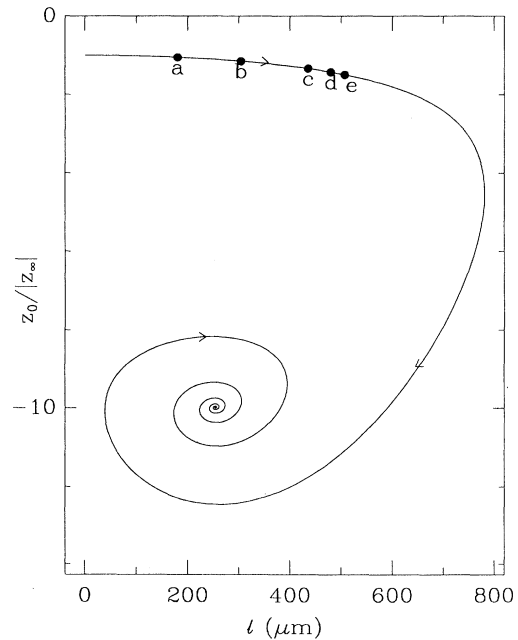

FIG. 2. Trajectory in the $(z_0/|z_\infty|,l)$ plane for the boundary-layer model with $v_p=10$ μm/s. Here z_0 is the position of the interface and l is the thickness of the boundary layer. We have also indicated the times a–e along the trajectory. Time a corresponds to 10 s, b to 30 s, c to 70 s, d to 90 s, and e to 105 s. Point e identifies the crossover from linear instability of the flat interface to nonlinear dendritic behavior.

oscillation becomes so large that it drives l all the way back to zero, at which point our approximation (2.10) ceases to be valid. Fortunately, we are concerned only with the early portion of our trajectories (as we show later), which are well defined for all velocities, and therefore we do not need to worry about this unphysical consequence of the approximation (2.10).

III. ONSET OF INSTABILITY

Our next job is to examine the morphological stability of the accelerating flat interface. For this purpose, it is simplest to work in a frame of reference moving with the interface. That is, we write (in the gradient frame) $c(\mathbf{x},z,t)=c[\mathbf{x},z-z_0(t),t]$, so that the diffusion equation becomes

$$D\nabla^2 c + v_0\frac{\partial c}{\partial z'} = \frac{\partial c}{\partial t} , \qquad (3.1)$$

where $z'=z-z_0$ and, as before, $v_0=v_p+\dot{z}_0$. We now allow variations in the $\mathbf{x}$ plane perpendicular to the growth direction. For the situations being considered here, we expect the initial instabilities of the flat interface to occur on length scales smaller than the thickness of the sample, that is, smaller than the spacing between the glass plates. Thus $\mathbf{x}$ must be a fully two-dimensional variable.

Suppose the interface is at $z=z_s(\mathbf{x},t)=z_0(t)+z_s'(\mathbf{x},t)$. Denote the value of the solute concentration at the interface by $c_s(\mathbf{x},t)$. Local thermodynamic equilibrium at the interface requires

$$c_s = -\frac{G}{m}z_s - d_0\mathcal{H}_s . \qquad (3.2)$$

Here $\mathcal{H}_s$ is the curvature of the interface, and d_0 is the capillary length,

$$d_0 = \frac{\gamma T_0}{Lm} , \qquad (3.3)$$

where L is the latent heat per unit volume. Conservation of solute at the interface implies

$$-D\frac{\partial c}{\partial z'}\bigg|_{z_s'} = (v_p+\dot{z}_s)(1-K)c_s . \qquad (3.4)$$

To carry out a linear stability analysis, we write

$$c(\mathbf{x},z,t)=c_0(z,t)+\delta c_k(z,t)e^{i\mathbf{k}\cdot\mathbf{x}} , \qquad (3.5)$$

and

$$z_s(\mathbf{x},t)=z_0(t)+z_k(t)e^{i\mathbf{k}\cdot\mathbf{x}} , \qquad (3.6)$$

where the functions c_0 and z_0 are the time-dependent concentration profile and the position of the planar interface that were computed approximately in Sec. II. Note that for this portion of the calculation, we may treat c_0 and z_0 as the exact solution to the flat interface problem, as the results are independent of the approximations used in Sec. II. A fully exact procedure for our stability calculation would involve linearizing (3.1), (3.2), and (3.4) in c_k and z_k and solving the resulting differential equations. If the acceleration of the planar interface is sufficiently

slow, however, we may be able, temporarily, to ignore the time dependence of c_0 and z_0 while we carry out a conventional Mullins-Sekerka stability calculation [3]. That is, we write

$$\delta c_k(z',t)\approx e^{-q_k z'}c_k(t), \quad \frac{dc_k}{dt}=\omega_k(t)c_k , \qquad (3.7)$$

$$\frac{dz_k}{dt}=\omega_k(t)z_k , \qquad (3.8)$$

and then compute the amplification rate ω_k and inverse decay length q_k as functions of the slowly time-dependent quantity z_0. Note that the only quantity for which we assume a slow time dependence, in order to perform the Mullins-Sekerka calculation, is q_k. The accuracy of this procedure is uncertain, and a more careful treatment may eventually be needed.

Inserting (3.7) into the diffusion equation (3.1), we obtain

$$\omega_k = D(q_k^2-k^2)-q_k v_0 . \qquad (3.9)$$

Note that we are not assuming quasistationarity; that is, we are not setting $\omega_k=0$ in (3.9) as is frequently done in the steady-state analysis. The boundary conditions (3.2) and (3.4) yield a second relation which we can write in the form

$$q_k\left[D+(1-K)v_0z_0+\frac{Dd_0k^2m}{G}\right]$$
$$=\dot{z}_0+(1-K)\left[\frac{v_0^2z_0}{D}+\omega_kz_0+v_0+\frac{d_0v_0k^2m}{G}\right] . \qquad (3.10)$$

The above result may be put in a more familiar form by employing our boundary-layer calculation from Sec. II and using (2.11) to write $v_0z_0(1-K)=2D/l(z_0-z_\infty)$ to find

$$q_k\left[1+\frac{2}{l}(z_0-z_\infty)+\frac{d_0k^2m}{G}\right]$$
$$=\frac{\dot{z}_0}{D}+\frac{2}{l}(z_0-z_\infty)\left[\frac{v_0}{D}+\frac{\omega_k}{v_0}+\frac{1}{z_0}+\frac{d_0k^2m}{Gz_0}\right] . \qquad (3.11)$$

Eliminating q_k from these equations and inserting the values of z_0 and l obtained from our previous calculation, we can compute a time-dependent spectrum of amplification rates $\omega_k(t)$.

We now must address one of the most difficult issues that arises in problems of this kind. In order to determine when and in what form the instabilities just described make themselves apparent in an experiment, we must specify how they are initiated. The natural assumption is that the triggering mechanism is simply the action of ambient thermodynamic fluctuations in the solidifying liquid. This is, in fact, quite a remarkable assumption—that microscopic atomic-scale irregularities are so

dramatically amplified by the instabilities that they produce macroscopically observable patterns. This assumption has been tested in other related situations, for example, as an explanation for dendritic sidebranches [4] and as a theory of the onset of hydrodynamic instabilities [5]. In most cases, the strength of purely thermal fluctuations appears somewhat small to explain the observed phenomena; but elements of the theory remain uncertain and the apparent discrepancies generally do not seem large enough to require the explicit introduction of alternative noise sources as essential ingredients of realistic models.

In principle, we would like to derive and solve a stochastic version of (3.8)

$$\frac{dz_k}{dt} = \omega_k(t)z_k + \eta_k(t) , \qquad (3.12)$$

where $\eta_k(t)$ is a fluctuating force whose statistical properties ought to be deducible from thermodynamic considerations. The formal solution of (3.12) is

$$z_k(t) = \int_{-\infty}^{t} dt' \exp\left[\int_{t'}^{t}\omega_k(t'')dt''\right]\eta_k(t') . \qquad (3.13)$$

We use the term "formal" because, in all likelihood, the stochastic forces η_k depend on the state variables z_k, c_k, etc., especially under strongly nonequilibrium situations such as this one.

Rather than tackle this problem in all its theoretical subtlety, we proceed as follows. Suppose that the η_k are statistically distributed in such a way that

$$\langle \eta_k(t)\eta_{k'}(t')\rangle = \Gamma_0(k)(2\pi)^2\delta^2(\mathbf{k}+\mathbf{k}')\delta(t-t') , \qquad (3.14)$$

where the angular brackets denote an average over the ensemble of fluctuations η_k. Let us further assume, despite our expectation to the contrary, that $\Gamma_0(k)$ is state independent and therefore independent of time t. Then

$$\langle z_k(t)z_{k'}(t)\rangle \approx \Gamma_0(k)(2\pi)^2\delta^2(\mathbf{k}+\mathbf{k}')$$
$$\times \int_{-\infty}^{t} dt_1 \exp\left[2\int_{t_1}^{t}\omega_k(t'')dt''\right] . \qquad (3.15)$$

For times $t<0$, before the pulling speed has been changed from zero to v_p, the system is in stable equilibrium, that is, $\omega_k(t<0) \equiv \omega_k^{(eq)} < 0$ for all k, and

$$\langle z_k(t)z_{k'}(t)\rangle = (2\pi)^2\delta^2(\mathbf{k}+\mathbf{k}')\Gamma_0(k)\frac{1}{2|\omega_k^{(eq)}|}$$
$$\equiv \langle z_k z_{k'}\rangle_{\text{equil}} . \qquad (3.16)$$

This is a quantity that we can calculate with some confidence. The $\omega_k^{(eq)}$ can be obtained from (3.9) and (3.10) simply by setting $v_0=0$ and $z_0=z_\infty$; thus, if we can compute $\langle z_k z_{k'}\rangle_{\text{equil}}$, we can evaluate $\Gamma_0(k)$, and then we can use this result to compute the amplification of fluctuations in (3.15).

The technique for calculating the morphological fluctuations of a solidification front at or near equilibrium was first described by Cherapanova [6] and later developed by one of us [4]. The idea is to add a Langevin force to the diffusion equation for the solute concentration c, and then to calculate the linear response of the de-

formations z_k to this force. The Langevin term is chosen so as to reproduce the known fluctuations of c in an infinite system in thermodynamic equilibrium. In doing this, we are ignoring the effect of the boundary upon the Langevin force, which is equivalent to performing the calculation in the so-called "symmetric model" [7]. These calculations are straightforward but cumbersome, and need not be reproduced in detail here. (A more correct calculation using the "one-sided model" seems unnecessarily complicated for present purposes.) The result that we need is

$$\langle \hat{z}_{K_1\Omega_1}\hat{z}_{k_2\Omega_2}\rangle_{\text{equil}} = \left[\frac{m}{G}\right]^2\frac{c_\infty}{Dn_\infty}(2\pi)^3\delta^2(k_1+k_2)$$
$$\times\delta(\Omega_1+\Omega_2)\text{Re}[f(k_1,\Omega_1)] , \qquad (3.17)$$

where $\hat{z}_{k\Omega}$ is the time Fourier transform of $z_k(t)$, Ω is the corresponding frequency, n_∞ is the total number of molecules per unit volume in the fluid, Re indicates the real part, and

$$\frac{1}{f(k,\Omega)} = \left[\left[1+\frac{md_0}{G}k^2\right]\left[k^2-\frac{i\Omega}{D}\right]^{1/2}\right.$$
$$\left. -\frac{i(1-K)mc_\infty\Omega}{\{2\}DG}\right]\left[1+\frac{md_0}{G}k^2\right] . \qquad (3.18)$$

Because $f(k,\Omega)$ is proportional to a response function, we except that it should have a pole in the Ω plane at $\Omega = -i\omega_k^{(eq)}$, which is almost, but not quite, true because we have used the symmetric model. We may correct this problem (albeit in a nonrigorous fashion) without changing the basic structure of the expression, by eliminating the factor of 2 in curly brackets in (3.18) so that the pole occurs at the correct point. Thus, we write

$$\frac{1}{f(k,\Omega)} \rightarrow \left[\left[1+\frac{md_0}{G}k^2\right]\left[k^2-\frac{i\Omega}{D}\right]^{1/2}\right.$$
$$\left. -\frac{i(1-K)mc_\infty\Omega}{DG}\right]\left[1+\frac{md_0}{G}k^2\right] . \qquad (3.19)$$

Combining (3.16) and (3.17), we have

$$\Gamma_0(k) = \left[\frac{m}{G}\right]^2\frac{c_\infty}{Dn_\infty}2|\omega_k^{(eq)}|\int\frac{d\Omega}{2\pi}\text{Re}[f(k,\Omega)]$$
$$= |\omega_k^{(eq)}|\frac{m}{(1-K)Gn_\infty A(k)} , \qquad (3.20)$$

where

$$A(k) = 1+\frac{md_0}{G}k^2 . \qquad (3.21)$$

We are finally able to answer several physically important questions: At what point in the development of the instabilities on the planar interface do deformations become observable? What is the characteristic wavelength of the deformation for which this happens? At what point do these deformations begin to behave in an intrin-

sically nonlinear manner; that is, when does the system cross over from smooth sinusoidal deformations to cellular or dendritic behavior?

The answers to the first and third of these questions are essentially the same: The deformations become both visible and nonlinear when their amplitude becomes roughly comparable to their wavelength. Thus, we calculate

$$\langle \delta z^2(t) \rangle \equiv \langle z_s'^2(\mathbf{x},t) \rangle = \int \frac{d^2k}{(2\pi)^2} \Gamma(k,t) , \qquad (3.22)$$

where from (3.15)

$$\Gamma(k,t) = \Gamma_0(k) \int_{-\infty}^{t} dt_1 \exp\left[2 \int_{t_1}^{t} \omega_k(t')dt'\right] . \qquad (3.23)$$

The function $\Gamma(k,t)$ is shown in Fig. 3 as a function of k for five different values of t. Relevant parameters are $v_p = 10$ μm/s, and $G = 67$ K/cm. The times shown are also indicated in Fig. 2 as points along the trajectory in the z_0, l plane. Clearly, long before the time at which the planar interface has reached steady state, Γ has become very strongly peaked in k, and the fluctuations in the neighborhood of this peak have been amplified by many orders of magnitude. Note also that the initial instability starts at relatively long wavelengths and moves to shorter ones as the solidification front accelerates.

According to the above discussion, the crossover wavelength occurs at $t = t_0$ when

$$\frac{2\pi}{k_{max}(t_0)} \equiv \lambda_0 \approx \langle \delta z^2(t_0) \rangle^{1/2} , \qquad (3.24)$$

where $k_{max}(t_0)$ is the value of k at the peak of Γ. Here we have identified $2\pi/k_{max}$ with the initial spacing observed by TS and shown in Fig. 1. The final approximate
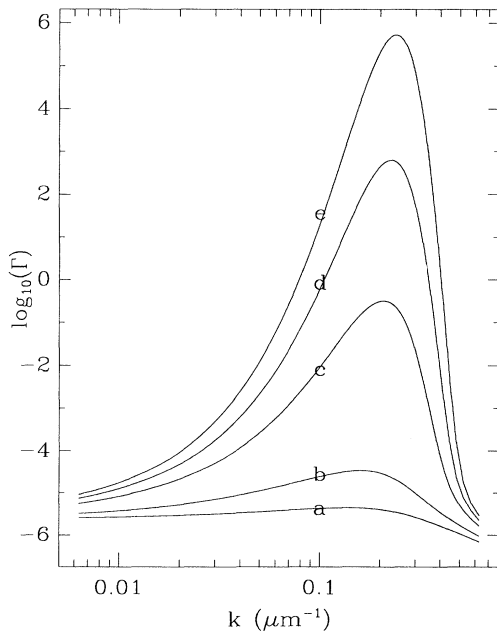
equality in (3.24) is correct only to within some multiplicative factor of order unity. Luckily, this factor is not very important. The amplitude $\langle \delta z^2(t) \rangle^{1/2}$ is increasing exponentially in time whereas k_{max} is changing relatively slowly and, as a result, λ_0 is not very sensitive to the precise choice of this factor.

Our numerical results for λ_0, along with the experimental observations of TS, are shown in Fig. 4 as functions of v_p. In obtaining these we have evaluated (3.23) numerically, and then made a Gaussian approximation for the peak in $\Gamma(k,t)$ in order to compute the integral in (3.22). This integral formally diverges unless one introduces a physically sensible cutoff. A choice of $k^{-1} \approx 3$ Å introduces negligible correction to our Gaussian approximation, and hence is justifiably ignored. For $v_p = 10$ μm/s in this figure, the crossover time is $t_0 = 105$ s, which is indicated by point "e" in Fig. 2. As advertised, the amplification occurs very early in the trajectories. The crossover time is also indicated in Fig. 3 by the curve marked "e." We see that the initial noise profile is amplified by approximately 11 orders of magnitude by the time it reaches the end of linearity; that is, the scale of the deformation is amplified by almost 10^6. Also shown in Fig. 4 are results obtained by TS by identifying λ_0 as the wavelength of the most rapidly growing instabilities for a steady-state flat interface moving at the pulling speed v_p. Obviously the latter analysis vastly underestimates λ_0 and does not even have the same qualitative dependence on v_p as the experimental data. Our own results predict λ_0 with surprising accuracy.

FIG. 3. Plots of $\Gamma(k,t)$ for $v_p = 10$ μm/s, where times labeled $a-e$ are the same as those in Fig. 2.
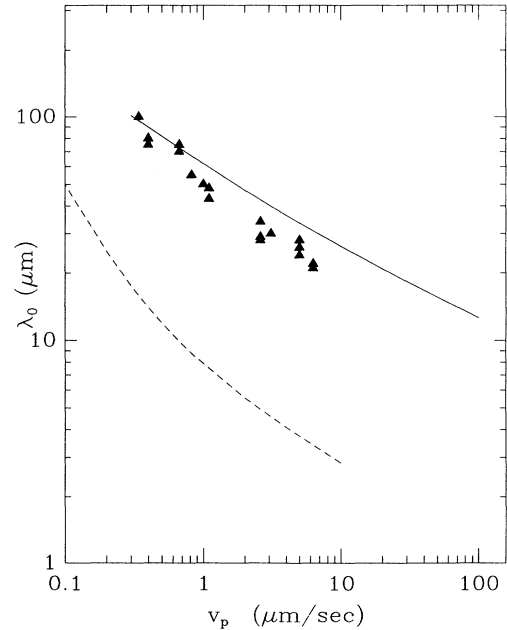

FIG. 4. Theoretical values of λ_0 (the solid line) vs the experimental values of TS (black triangles) and their calculation of the steady-state Mullins-Sekerka maximum wavelength (dashed line).

IV. DYNAMICS OF THE DENDRITIC ARRAY

Our strategy for the next part of this calculation is to use the parameters computed at the crossover point, λ_0 and z_0, as initial conditions for an array of dendrites whose average spacing at later times will be denoted $\lambda_1(t)$ and whose tips, on the average, will be at $\bar{z}(t)$ as measured in the gradient frame. Our problem, therefore, is to derive and then solve a pair of coupled equations of the form

$$\dot{\bar{z}} = V(\bar{z}, \lambda_1; v_p) \tag{4.1}$$

and

$$\dot{\lambda}_1 = \Lambda(\bar{z}, \lambda_1; v_p) , \tag{4.2}$$

where V and Λ are functions to be determined. These equations must describe, at least in some useful approximation, the way in which the dendritic tips compete with each other during growth, and the way in which this competition produces coarsening of the array, that is, an increase in λ_1. We expect to be able to integrate (4.1) and (4.2) forward in time and thus to predict the final steady-state configuration of the system.

In order to accomplish this task we modify our earlier steady state model [8] so that it applies at velocities $\dot{\bar{z}}$ not necessarily equal to the pulling speed. The required modification is very small, but it will be best for purposes of clarity to review briefly the basic ingredients of the calculation. More details can be found in Ref. [8].

Our starting point is the diffusion equation for the solute concentration in the gradient frame [9],

$$\frac{\partial c}{\partial t} - v_p \frac{\partial c}{\partial z} - D\nabla^2 c = \sum_i \mathscr{S}_i(\mathbf{r}, t) , \tag{4.3}$$

where $\mathscr{S}_i$ denotes the source strength associated with the ith dendrite, that is, the rate at which the solute is being rejected into the fluid at positions $\mathbf{r}$ along the solidification front. Equation (4.3) has the formal solution

$$c(\mathbf{r}, t) = c_\infty + \sum_i \int d\mathbf{r}' \int_{-\infty}^{t} dt' \mathscr{G}(\mathbf{r}, t|\mathbf{r}', t') \mathscr{S}_i(\mathbf{r}', t') , \tag{4.4}$$

where $\mathscr{G}$ is the Green's function for the operator on the left-hand side of (4.3).

Our strategy is to use Eq. (4.4) to write an equation of motion, not for the entire solidification front, but only for the positions $z_i(t)$ of the tips of the dendrites. To do this, we make a number of assumptions, specifically the following.

(1) *Quasistationarity.* We neglect the explicit time dependence of $\mathscr{S}_i$ in (4.4); however, $\mathscr{S}_i$ still depends implicitly on the time because it is a function of the instantaneous growth rate v_i, the position of the tip z_i, and the radius of curvature of the tip ρ_i.

(2) *Slender, three-dimensional dendrites.* The tip of each dendrite is assumed to be well separated both from all other tips and from the walls of the container.

(3) *Local equilibrium.* The concentration c_i at the position z_i of the ith tip is fixed by the liquidus on the phase diagram, that is,

$$c_i = -\frac{G}{m} z_i . \tag{4.5}$$

Note that we are omitting the Gibbs-Thomson correction here. Capillarity plays a role only in the next of these assumptions.

(4) *Solvability* or, equivalently for these purposes, "*marginal stability*" [10]. The instantaneous growth rate v_i of the ith tip is determined by a condition [11–13] of the form

$$\frac{2Dd_0}{(\Delta c_i) v_i \rho_i^2} = \sigma^* , \tag{4.6}$$

where the quantity $\Delta c_i = -(1-K)Gz_i/m$ is the jump in equilibrium concentration of solute between the solid and liquid phases at a temperature $T_0 + Gz_i$. We assume that σ^* is independent of the solutal Péclet number

$$p_i = \frac{\rho_i v_i}{2D} . \tag{4.7}$$

For the well-separated dendrites of interest to us p_i will be small, of order 10^{-2} or less, and the limit $p_i \to 0$ almost certainly is accurate enough for our purposes. (For succinonitrile, $\sigma^* \approx 0.04$.)

A more serious assumption, especially for growth conditions near the cell-to-dendrite transition, is that the solvability condition does not depend on the spacing λ_1. In general, we must expect that when λ_1 is less than the dynamic diffusion length $\bar{l} \equiv 2D/\bar{v}$, the dendritic tips will interact so strongly with each other that their shapes will be deformed and, therefore, the solvability mechanism for velocity selection will be significantly altered. In short, we are making the strong assumption that the properties of any dendritic tip in our array are the same as those of an isolated dendrite growing slowly in a homogeneous melt. The condition $\lambda_1 > \bar{l}$ is an important limitation on the validity of our calculation.

The next step is to evaluate each term in Eq. (4.4) for a value of $\mathbf{r}$ near the tip of, say, the ith dendrite. Consider first the contribution δc_{ij} to the sum in (4.4) from the jth dendrite with $j \neq i$. According to assumption (2), the region near the tip of this dendrite should look like a one-dimensional source of solute when observed from distances of order $\lambda_1 \gg \rho_j$. After some calculation we find

$$\delta c_{ij} = \frac{Gp_j(1-K)}{m} \left[\frac{l_p}{2} \left[1 - \frac{\lambda_{ij}^2}{l_p d_{ij}} \right] \exp\left[-\frac{d_{ij}}{2l_p} \right] \right.$$
$$\left. - \left[z_i - \frac{\lambda_{ij}^2}{2l_p} \right] E_1\left[\frac{d_{ij}}{l_p} \right] \right] , \tag{4.8}$$

where $l_p = 2D/v_p$; λ_{ij} is the distance, in the plane perpendicular to the growth direction, between the ith and jth dendrites; $d_{ij} = z_{ij} + [\lambda_{ij}^2 + z_{ij}^2]^{1/2}$; $z_{ij} = z_i - z_j$; and E_1 is the exponential integral

$$E_1(x) = \int_x^\infty \frac{e^{-t}}{t} dt . \tag{4.9}$$

Approximating $\mathscr{S}_i$ by a line source is not appropriate for the term δc_{ii}, where the point $\mathbf{r}$ at which $c(\mathbf{r})$ is being evaluated is the tip of the same paraboloidal surface from which solute is being rejected. In this case, we find

$$\delta c_{ii} = \frac{G(1-K)p_i}{m}\left[\frac{l_p}{2}\left[1+\frac{\rho_i}{l_p}\right]\right.$$
$$\left. -\left[z_i+\rho_i+\frac{\rho_i^2}{2l_p}\right]E_1\left[\frac{\rho_i}{l_p}\right]\right], \quad (4.10)$$

which is a generalization of the Ivantsov relation [14].

Combining the formal solution of the diffusion equation (4.4), evaluated at the tip of the ith dendrite, with the boundary condition (4.5) and the specific results (4.8) and (4.10), we find

$$\frac{z_i-z_\infty}{(1-K)} = p_i e^{\rho_i/l_p} E_1\left[\frac{\rho_i}{l_p}\right]\left[z_i+\rho_i+\frac{\rho_i^2}{2l_p}\right] - \frac{p_i}{2}(l_p+\rho_i)$$
$$+ \sum_{j\,(\neq i)} p_j\left[\left[z_i-\frac{\lambda_{ij}^2}{2l_p}\right]E_1\left[\frac{d_{ij}}{l_p}\right] - \frac{l_p}{2}\left[1-\frac{\lambda_{ij}^2}{l_p d_{ij}}\right]\exp\left[-\frac{d_{ij}}{l_p}\right]\right]. \quad (4.11)$$

Here it is useful to remember that the velocities v_i which occur in the Peclét numbers p_i are related to z_i via

$$v_i = v_p + \frac{dz_i}{dt}. \quad (4.12)$$

Our calculation so far has been identical to Ref. [8]. Our first deviation from Ref. [8] comes in writing our results for a uniform array that is not necessarily at steady state. For the uniform case, all our velocities v_i (which in turn measure the strengths of the various tip sources) are not equal to v_p but instead are equal to the instantaneous array velocity $\bar{v}(t)$. This small modification yields

$$\frac{\bar{z}-z_\infty}{(1-K)} = \bar{p}e^p E_1(p)\left[\bar{z}+\rho+\frac{\rho p}{2}\right] - \frac{\bar{p}}{2}(l_p+\rho) + \bar{p}\sum_{\substack{i,j\\(i\neq j)}}\left[\left[\bar{z}-\frac{\lambda_{ij}^2}{2l_p}\right]E_1\left[\frac{\lambda_{ij}}{l_p}\right] + \frac{l_p}{2}\left[\frac{\lambda_{ij}}{l_p}-1\right]\exp\left[-\frac{\lambda_{ij}}{l_p}\right]\right], \quad (4.13)$$

where

$$\bar{p} = \frac{\rho}{\bar{l}}, \quad \bar{l} = \frac{2D}{\bar{v}}. \quad (4.14)$$

In steady state we have $\bar{p}\to p$, therefore

$$p = \frac{\rho}{l_p}. \quad (4.15)$$

In the same fashion, the solvability condition (4.6) is modified to read

$$-\frac{3D\gamma T_0}{(1-K)LG\bar{v}\rho^2\bar{z}} = \sigma^*. \quad (4.16)$$

Equation (4.16) determines ρ as a function of $\bar{z}$ and $\dot{\bar{z}}$, for fixed v_p, and we can use this relation to eliminate ρ from all other expressions. If this elimination is performed in (4.13) we obtain $\dot{\bar{z}}$ as a function of $\bar{z}$ and λ_1, which is precisely the type of equation that we were seeking at the outset of this section. The condition $\dot{\bar{z}}=0$ implies steady state, and it is easy to check that this steady state is a stable attractor for fixed λ_1.

Having now found one of our equations of motion, we have yet to determine the expression governing the evolution of λ_1. We do this by studying the stability of the non-steady-state dendritic array, again using the same methods that we developed in Ref. [8] for the steady-state situation.

To study linear stability, we linearize (4.11) about the uniform solution described by (4.13), and assume that all small departures from steady state grow (or decay) with an amplification rate ω. For example,

$$z_i - \bar{z} = \delta z_i e^{\omega t}, \quad v_i - \bar{v} = \omega \delta z_i e^{\omega t}, \quad (4.17)$$

etc. Then, from the solvability condition (4.6), we find

$$\delta p_i = -\frac{\bar{p}}{2}\left[\frac{1}{z} - \frac{\omega}{\bar{v}}\right]\delta z_i \quad (4.18)$$

and

$$\delta \rho_i = -\frac{\rho}{2}\left[\frac{1}{\bar{z}} + \frac{\omega}{\bar{v}}\right]\delta z_i. \quad (4.19)$$

Ultimately, we find results quite similar to the steady-state results of Ref. [8], namely an equation of the form

$$\omega \sum_j A_{ij}\delta z_j = \sum_j B_{ij}\delta z_j. \quad (4.20)$$

Here

$$A_{ij} = A^{(0)}\delta_{ij} + (1-\delta_{ij})A_{ij}^{(1)},$$
$$B_{ij} = B^{(0)}\delta_{ij} + (1-\delta_{ij})B_{ij}^{(1)}, \quad (4.21)$$

with

$$A^{(0)} = \frac{1}{2\bar{v}}\left\{e^p E_1(p)\left[(1-p)\left[\bar{z}+pl_p+\frac{p^2 l_p}{2}\right] - pl_p(1+p)\right] + \left[\bar{z}+pl_p+\frac{p^2 l_p}{2}-\frac{l_p}{2}\right]\right\}, \quad (4.22)$$

$$A_{ij}^{(1)} = \frac{1}{2\bar{v}} \left[\left[\bar{z} - \frac{\lambda_{ij}}{2l_p} \right] E_1 \left[\frac{\lambda_{ij}}{l_p} \right] + \tfrac{1}{2}(\lambda_{ij} - l_p) \exp \left[-\frac{\lambda_{ij}}{l_p} \right] \right] , \tag{4.23}$$

$$B^{(0)} = \frac{1}{(1-K)\bar{p}} - e^p E_1(p) - p \sum_{\substack{i,j \\ (i \neq j)}} \left[E_1 \left[\frac{\lambda_{ij}}{l_p} \right] - \frac{\bar{z}}{\lambda_{ij}} \exp \left[-\frac{\lambda_{ij}}{l_p} \right] \right]$$

$$+ \frac{1}{2\bar{z}} \left[e^p E_1(p)(1+p) \left[\bar{z} + 2pl_p + \frac{p^2 l_p}{2} \right] - \left[\bar{z} + 2pl_p + \frac{p^2 l_p}{2} + \frac{l_p}{2} \right] \right] , \tag{4.24}$$

$$B_{ij}^{(1)} = \frac{1}{2\bar{z}} \left[\left[\bar{z} - \frac{\lambda_{ij}^2}{2l_p} \right] E_1 \left[\frac{\lambda_{ij}}{l_p} \right] + \tfrac{1}{2}(\lambda_{ij} - l_p) \exp \left[-\frac{\lambda_{ij}}{l_p} \right] \right] - \frac{\bar{z}}{\lambda_{ij}} \exp \left[-\frac{\lambda_{ij}}{l_p} \right] . \tag{4.25}$$

Fourier transformation of (4.20) (in the array index i) yields the spectrum of amplification rates

$$\omega(\mathbf{q}) = \frac{\hat{B}(\mathbf{q})}{\hat{A}(\mathbf{q})} . \tag{4.26}$$

The only change in the above from Ref. [8] is in the replacement of p by $\bar{p}$ and v_p by $\bar{v}$ at several points in the expressions. We already understand how $\omega(\mathbf{q})$ behaves for a variety of $\bar{z}$, v_p, and λ_1 when $\dot{\bar{z}}=0$. It is useful to find out if there is a significant change as $\dot{\bar{z}}$ varies from $-v_p$ (stationary in the material frame) to $\dot{\bar{z}}=0$ (moving at the pulling speed). In Fig. 5 we examine $\omega(\mathbf{q})$ for fixed values of λ_1, $\bar{z}$, and v_p, and we allow $\dot{\bar{z}}$ to have three different values. The results seem physically sensible. For $\dot{\bar{z}}=-50$ μm/s our system is stable, for $\dot{\bar{z}}=0$ μm/s, it is marginally stable, while for $\dot{\bar{z}}=100$ μm/s it is unstable.
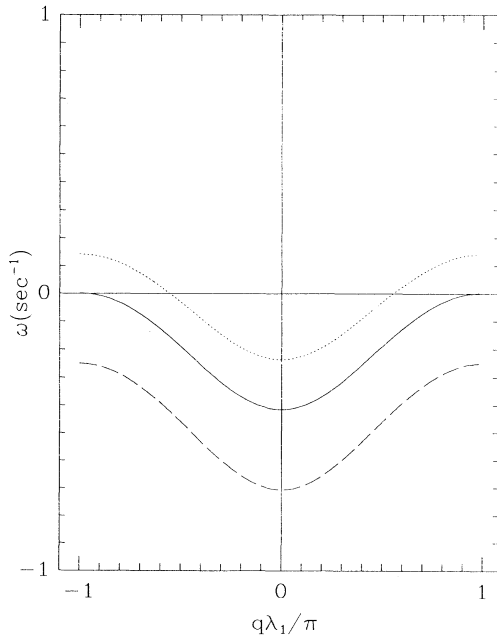

FIG. 5. Amplification rates $\omega(\mathbf{q})$ for fixed values of $\lambda_1 = 59.2$ μm and $v_p = 100$ μm/s. The unstable curve occurs for $\dot{\bar{z}}=100$ μm/s, the marginally stable curve for $\dot{\bar{z}}=0$ μm/s, and the overstable curve for $\dot{\bar{z}}=-50$ μm/s.

But perhaps most significantly, for our purposes, is that the maximum in $\omega(\mathbf{q})$ persists at $\mathbf{q} = (\pi/\lambda_1)\hat{e}_x \equiv q_{max}$.

This wave number q_{max} corresponds to the instability in which every other dendrite grows at the expense of its nearest neighbor. That is, very roughly, the rate at which every other dendrite in the array is being overgrown by its neighbors and falling out of the front of the array. We therefore interpret ω_{max} as a doubling rate, and write

$$\dot{\lambda}_1 \approx \beta \omega_{max} \lambda_1 \quad \text{for } \omega_{max} > 0 , \tag{4.27}$$

where β is some constant of order unity. Equation (4.27) makes sense when $\omega_{max} > 0$; the coarsening instability that we are considering allows only $\dot{\lambda}_1 > 0$. Accordingly, we assume that when $\omega_{max} < 0$, $\dot{\lambda}_1 = 0$.

This hypothesis, along with our results in Eqs. (4.13)–(4.16), produces the desired pair of nonlinear first-order differential equations describing the evolution of $\bar{z}$ and λ_1. However, we must take our equation for $\dot{\lambda}_1$ with more than a few grains of salt, as it is far from encompassing all of the physics of our system. We have ignored phenomena such as tip splitting, the growth of tertiary arms along the dendrites [both of which would allow for reduction in wavelength), i.e., $\dot{\lambda}_1 < 0$], and perhaps other mechanisms for coarsening. Although we have omitted a great deal, it is probably fair to say that what we have postulated is some sort of rough estimate for the coarsening process. Probably it is the best we can do at this point.

Now that we have found our equations for $\dot{\bar{z}}$ and $\dot{\lambda}_1$ we should be able to evolve our array forward from an initial state. But, before we perform this evolution, we must ask whether the wavelengths λ_0 computed in Sec. III are sensible initial conditions for our dendrite model. If they are not, we will need to extend our mode amplification model into the cellular regime, as is discussed in Ref. [15]. Since the basic quantitative measure of whether a system is likely to be in the dendritic regime of growth is whether $\lambda_1 \gtrsim \bar{l}$ (where our approximation of weakly coupled dendrites is valid) we may use as initial conditions those states for which $\lambda_0 \gtrsim \bar{l}$. This condition is either met or nearly met for all pulling speeds for which we are able meaningfully to characterize the final steady state using the work of Ref. [8].

A typical trajectory in the $\lambda_1, \bar{z}$ plane based on solutions to (4.1) and (4.2), for a pulling speed of $v_p = 65.6$ μm/s, is shown in Fig. 6. The initial point is la-

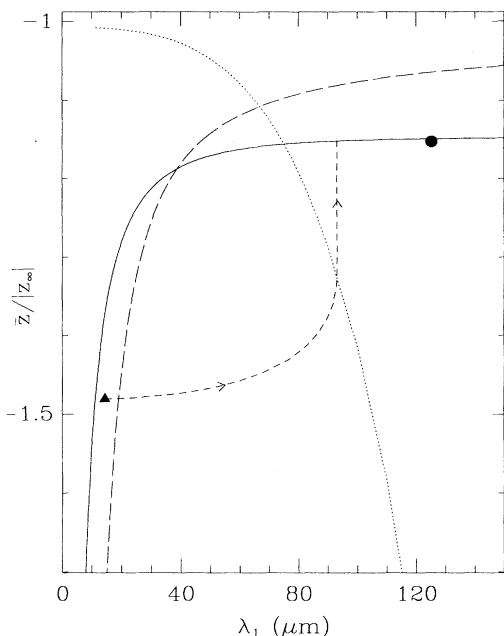FIG. 6. A full trajectory for a dendritic array (the short-dashed curve) with $v_p = 65.6$ μm/s, starting at the crossover point determined by the boundary-layer model (the black triangle) and ending at a stable fixed point on the $\dot{\bar{z}}=0$ curve (solid line). The long-dashed curve indicates the locus of points where $\lambda_1 = \bar{l}$. The intersection of the $\dot{\lambda}_1 = 0$ curve (dotted) with the $\dot{\bar{z}}=0$ curve (solid) defines the neutrally stable configuration of the array. The black circle is the experimental result of SMT.
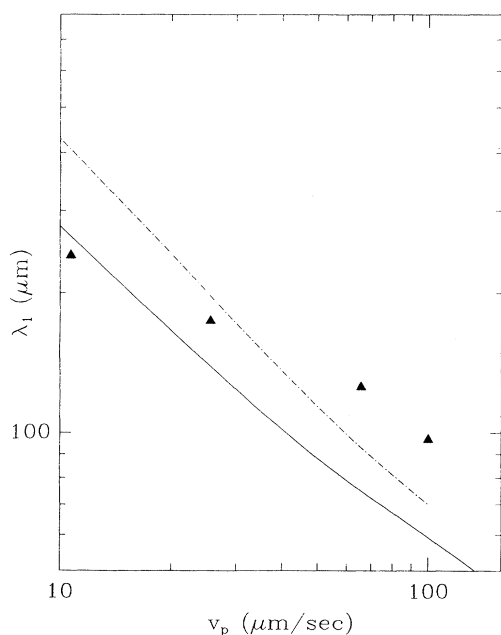

FIG. 7. A plot of our final wavelength (the dot-dashed line) compared with the experimental data from SMT (the solid triangles). The solid line is the neutral stability curve [$\omega(k_m)=0$].

beled by a dark triangle, and we see by its position relative to the $\lambda_1 = \bar{l}$ curve (long-dashed) that it is not quite inside the regime where $\lambda_0 = \lambda_1(t=0) > \bar{l}$, but is close enough, given the roughness of this criterion. The intersection of the $\dot{\bar{z}}=0$ curve (solid) with the $\dot{\lambda}_1 = 0$ curve (dotted) defines the marginally stable solution for the steady-state dendritic array, which was computed in Ref. [8]. The trajectory is indicated by the short-dashed curve emanating from the black triangle and terminating on the $\dot{\bar{z}}=0$ curve. Note that the system reaches a stable primary spacing well before arriving at the pulling speed, a phenomenon also observed by TS. The black circle is the experimental point from SMT, and the agreement is quite good for this pulling speed.

Figure 7, the culmination of this paper, is a plot of our new theoretical final wavelengths compared to the stability boundary computed in Ref. [8] and the experimental points of Somboonsuk, Mason, and Trivedi [2]. The agreement between theory and experiment is good only at the higher pulling speeds. Considering the complexity of the calculation, however, and the fact that we have allowed ourselves no adjustable parameters, we find this degree of agreement to be quite encouraging.

V. SUMMARY AND CONCLUSIONS

In the calculation described here, we have attempted—with some success—to follow the formation of a dendritic array all the way from the initial instability of a planar solidification front to the selection of a final steady-state primary spacing. Each stage of this calculation involves approximations and theoretical assumptions that deserve closer attention, specifically:

(1) The formation of the initial pattern of deformations of the planar front depends sensitively on the way in which this front and its accompanying diffusive boundary layer respond to the abrupt onset of motion of the imposed temperature gradient. We have used a rudimentary boundary-layer model to describe this process, and we suspect that any inaccuracies in this model are responsible for the fact that our predicted crossover wavelength λ_0 is slightly larger than that seen experimentally. In particular, we suspect that a more accurate calculation would perform better at higher velocities.

(2) Unlike the situation in Ref. [4], for example, where thermal fluctuations seemed to be too small to account for observed effects, the thermal noise in this case seems easily large enough to explain the strength of the instability that determines λ_0. Our calculation of the effects of thermal fluctuations contains several approximations, at least one of which is of a very fundamental nature. Improving this calculation will require the development of new techniques in nonequilibrium statistical mechanics, which is an important project for the future. We suspect, however, that any discrepancies are most likely to be explained by an improved boundary-layer calculation as mentioned in (1) above.

(3) By assuming only weak interactions between our dendritic tips, from the moment that they first appear at spacing λ_0 to their final coarsened configuration at spac-

ing λ_1, we have avoided a number of important problems that may need to be solved in extensions of this work. Specifically, our approximations are only valid at sufficiently large pulling speeds, and we have not even touched upon the possibility of cellular structures that might form at slower speeds or as intermediate stages in the formation of dendrites [15]. Also nothing that we have done would allow us to deal with situations in which the dendritic spacings might decrease via tip-splitting or higher-order side branching. Our coarsening model, based on stability of the weakly interacting array, is very crude, but at present we have no feasible improvement to suggest.

A number of extensions of the SMT experiments might be very useful in testing the accuracy of these various approximations and assumptions. It should be possible to check the location of the neutral stability curve in Fig. 7

simply by starting with well-formed steady-state arrays as obtained in the previous experiments and then decreasing the pulling speed gradually until further coarsening occurs. Also, it might be both possible and interesting to check more details of our calculation by direct observation of the time-dependent position of the planar front, $z_0(t)$, the mean position of the dendritic tips $\bar{z}(t)$, and the spacing $\lambda_1(t)$.

ACKNOWLEDGMENTS

*Present address: National Institute for Standards and Technology, Gaithersburg, MD 20899.

[1] R. Trivedi and K. Somboonsuk, Acta Metall. **33**, 1061 (1985).

[2] K. Somboonsuk, J. T. Mason, and R. Trivedi, Metall. Trans. A **15A**, 967 (1984).

[3] W. W. Mullins and R. F. Sekerka, J. Appl. Phys. **35**, 444 (1964).

[4] J. S. Langer, Phys. Rev. A **36**, 3350 (1987).

[5] G. Ahlers, M. C. Cross, P. C. Hohenberg, and S. Safran, J. Fluid Mech. **110**, 297 (1981).

[6] T. A. Cherapanova, Dokl. Akad. Nauk SSSR **226**, 1066 (1976) [Sov. Phys. Dokl. **21**, 109 (1976)].

[7] J. S. Langer and L. A. Turski, Acta. Metall. **25**, 1113 (1977).

[8] J. A. Warren and J. S. Langer, Phys. Rev. A **42**, 3518 (1990).

[9] One might be tempted to make a self-consistent approximation by writing the diffusion equation in the frame of reference that is moving at the mean velocity $\bar{v} = \dot{\bar{z}} + v_p$, but this would be a mistake. The mean velocity $\bar{v}$ is defined by the average over all tip positions z_i. Its use in the diffusion equation would, in effect, introduce an infinite-range interaction which would violate the quasi-stationarity approximation at the outset and cause difficulties in the stability analysis.

[10] J. S. Langer, Rev. Mod. Phys. **52**, 1 (1980).

[11] J. S. Langer, *Chance and Matter,* edited by J. Souletie, J. Vannimenus, and R. Stora, Lectures on the Theory of Pattern Formation, Les Houches Summer School, 1986 (North-Holland, New York, 1987), pp. 629–711.

[12] D. Kessler, J. Koplik, and H. Levine, Adv. Phys. **37**, 255 (1988).

[13] *Dynamics of Curved Fronts,* edited by P. Pelcé (Academic, New York, 1988).

[14] G. P. Ivantvsov, Dokl. Akad. Nauk. SSSR **58**, 567 (1947).

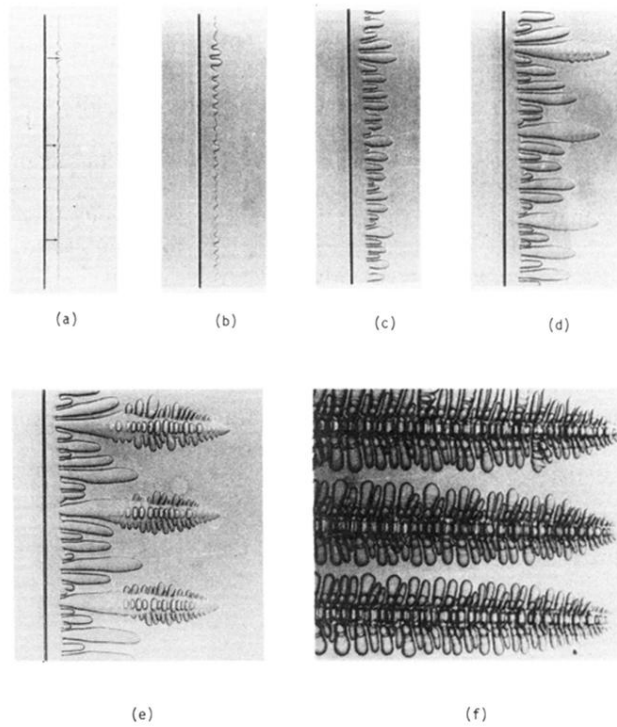[15] J. Warren, Ph.D. thesis, University of California, Santa Barbara, 1992 (unpublished).

FIG. 1. Sequence of photographs taken from TS illustrating the instability of a planar interface and the subsequent development of a steady-state dendritic array. (Reprinted from R. Trivedi and K. Somboonsuck, Acta Metall. **33**, 1061, copyright 1985, with permission from Pergamon Press Ltd., Headington Hill Hall, Oxford OX3 0BW, U.K.)